Trends in Analytical Chemistry 122 (2020) 115721

Contents lists available at ScienceDirect

Trends in Analytical Chemistry

journal homepage: www.elsevier.com/locate/trac

Synchrotron-based techniques for studying the environmental health effects of heavy metals: Current status and future perspectives

Huaiqiang Hu [a], Jiating Zhao [b, c], Liming Wang [b, c], Lihai Shang [d, **], Liwei Cui [e], Yuxi Gao [b, c], Bai Li [b], Yu-Feng Li [b, c, *]

[a] Department of Neurology, No. 960 Hospital of Chinese PLA, Jinan 250031, Shandong, China
[b] CAS Key Laboratory for Biological Effects of Nanomaterials and Nanosafety, HKU-IHEP Joint Laboratory on Metallomics, State Environmental Protection Engineering Centre for Mercury Pollution Prevention and Control, Institute of High Energy Physics, Chinese Academy of Sciences, Beijing 100049, China
[c] University of Chinese Academy of Sciences, Beijing 100049, China
[d] State Key Laboratory of Environmental Geochemistry, Institute of Geochemistry, Chinese Academy of Sciences, Guiyang 550002, China
[e] State Environmental Protection Engineering Centre for Mercury Pollution Prevention and Control, Beijing Advanced Sciences and Innovation Centre, Chinese Academy of Sciences, Beijing 101407, China

ARTICLE INFO

Article history:
Available online 9 November 2019

Keywords:
Synchrotron radiation
Quantification
Speciation
Mapping
Spatial speciation
Structure characterization
Heavy metals

ABSTRACT

This review summarizes the state-of-the-art synchrotron-based techniques for studying the environmental health effects of heavy metals exposure. Synchrotron radiation based X-ray fluorescence (SRXRF) is widely applied in quantification of metals in different biological and environmental samples. X-ray absorption spectrometry (XAS) is used for speciation of heavy metals. With high energy resolution fluorescence detected (HERFD) XAS, it is possible to study heavy metals in biological samples at realistic concentrations. The focused synchrotron-based X-ray is applied to image metals down to nm resolution at 2- or 3- dimension (2D or 3D). The combination of XAS with SRXRF can realize 2D or 3D spatial speciation, along with other techniques like scanning transmission X-ray microscopy (STXM) and full field XAS. The structure of metal-binding biomolecules can be characterized by Protein X-ray Diffraction (PX) and/or XAS, together with neutron scattering. The future aspects of multimode detection, new imaging methods, fast detector technologies and big data strategies in synchrotron-based techniques were also discussed.

1. Introduction

Environmental health science is a transdisciplinary field, which tackles public health threats from environmental exposures and estimate the magnitude of health risks related to environmental contaminants by investigating the mechanisms of biological response, and use this information to develop solutions to mitigate environmental problems [1]. Heavy metals are one of the many environmental exposure factors, which are metallic elements that have a density over 4.0 or 5.0 g/cm^3. Metalloids, such as arsenic, can also induce toxicity at low level of exposure, which are regarded as heavy metals, too [2,3]. Although heavy metals are naturally occurring, most heavy metals come from anthropogenic activities like mining, smelting, industrial production and domestic and agricultural application [4].

Many heavy metals play vital roles in the chemistry of life. For example, copper serves as a cofactor in many redox enzymes like Cytochrome C oxidase, which influence respiratory electron transport chain of mitochondria [5]. On the other hand, many heavy metals including those essential metals are toxic to living organisms at high concentrations. For example, lead, arsenic, manganese and methylmercury (MeHg) cause injury to the nervous system in humans [6]. The toxicity of heavy metals to organisms and human is highly linked to their concentration, speciation and distribution. Therefore, the study on the absorption, distribution, metabolism and excretion of heavy metals in biological systems will help us to understand the mechanisms underlying their environmental health effects.

* Corresponding author. CAS Key Laboratory for Biological Effects of Nanomaterials and Nanosafety, HKU-IHEP Joint Laboratory on Metallomics, State Environmental Protection Engineering Centre for Mercury Pollution Prevention and Control, Institute of High Energy Physics, Chinese Academy of Sciences, Beijing 100049, China.
** Corresponding author.
E-mail addresses: shanglihai@vip.skleg.cn (L. Shang), liyf@ihep.ac.cn (Y.-F. Li).

https://doi.org/10.1016/j.trac.2019.115721
0165-9936/

Abbreviations

AAS	Atomic Absorption Spectrometry
AFS	Atomic Fluorescence Spectrometry
EDX	Energy Dispersive X-Ray Fluorescence
EXAFS	Extended X-Ray Absorption Fine Structure
(HERFD) XAS	High Energy Resolution Fluorescence Detected X-Ray Absorption Spectrometry
ICP-MS	Inductively Coupled Plasma Mass Spectrometry
ICP-OES	Inductively Coupled Plasma Optical Emission Spectrometry
LA-ICP-MS	Laser Ablation Inductively Coupled Plasma Mass Spectrometry
MeHg	Methylmercury
NAA	Neutron Activation Analysis
NS	Neutron Scattering
PIXE	Proton-Induced X-Ray Emission
PM2.5	Fine Particulate Matter
PX	Protein X-Ray Crystallography
SIMS	Secondary Ion Mass Spectrometry
STXM	Scanning Transmission X-Ray Microscopy
SRXRF	Synchrotron Radiation Based X-Ray Fluorescence
WDX	Wavelength Dispersive X-Ray Fluorescence
XANES	X-Ray Absorption Near-Edge Structure
XAS	X-Ray Absorption Spectrometry

Different approaches have been applied to study the concentration, speciation and distribution of heavy metals [7–10]. Among all the techniques, synchrotron based techniques are versatile and sometimes indispensable to study the environmental health effects of heavy metals [11,12]. Synchrotron radiation (SR) is an advanced light source providing from infrared up to hard X-rays with high brilliance (many orders of magnitude more than conventional light sources) and pulsed light emission (pulse durations at or below one nanosecond). Synchrotron based techniques are developed through the interactions of synchrotron radiation with matters, i.e. absorption and scattering. Fourier transformed infrared spectroscopy (FTIR), X-ray absorption spectrometry (XAS), and X-ray computed tomography (X-CT), etc. are based on the absorption of synchrotron radiation by matters. X-ray diffraction (XRD), protein X-ray crystal diffraction (PX), and small angle X-ray scattering (SAXS) etc are based on the scattering of the synchrotron radiation. Besides, the detection of the emission of secondary particles like X-ray fluorescence spectrometry (XRF) and X-ray photoelectron spectroscopy (XPS), are also developed using synchrotron radiation [12,13].

The light produced by SR facility is highly polarized, tunable, and collimated, which make SR-based techniques outstanding tools in multidisciplinary research areas including physics, chemistry, life science, materials science, environmental science and environmental health science [14–17]. With the rapid growth in the number of SR facilities around the world, synchrotron-based techniques are more and more widely applied. To the best of our knowledge, there is no review focusing on the application of synchrotron based techniques for environmental health effects of heavy metals although there are references that summarized synchrotron based techniques like X-ray fluorescence imaging in biological systems [18]. This review summarizes the recent advances of synchrotron-based techniques in quantification, speciation, mapping, and spatial speciation of heavy metals and structure characterization of metal-binding biomolecules in environmental health study. Future aspects on the application of synchrotron based techniques to study the environmental health effects of heavy metals will also be discussed.

2. Multielemental quantification of heavy metals

Knowing the concentrations of heavy metals in biological systems is the first step to understand the environmental health effects of them. The quantification of heavy metals can be achieved through different element-specific techniques like atomic fluorescence spectrometry (AFS), atomic absorption spectrometry (AAS), etc, which are generally suitable for the determination of one or several specific metals in one run. Inductively coupled plasma optical emission spectrometry (ICP-OES) and inductively coupled plasma mass spectrometry (ICP-MS) can quantify multi-metals in one run with the detection limit as low as parts per trillion (ppt) level [19]. Most liquid and gaseous samples can be directly introduced into ICP-OES and ICP-MS, but solid samples need pretreatment like digestion or ashing, which is time-consuming, and may contaminate the samples. Neutron activation analysis (NAA) can measure more than 30 elements simultaneously in one run with the detection limits down to 10^{-6}– 10^{-13} g/g. In addition, NAA does not need sample digestion or dissolution and there is little opportunity for reagent or laboratory contamination. However, the radioactivity in the sample after neutron activation is the major concern for NAA, which requires qualified operation [9].

X-ray fluorescence analysis (XRF) is based on the detection of characteristic fluorescence after excitation by primary particle beam with sufficient energy. The intensity of the fluorescence measured by the detectors is proportional to the concentration of the element in the sample (Fig. 1). XRF is a non-destructive, multielemental analytical technique. The particle beam can be electrons (electron microscope-energy dispersive spectrometer, EM-EDS), an X-ray beam or a proton beam (proton induced X-ray emission, PIXE). The detection limit for commercial XRF (using X-ray tube) is around part per million (ppm) while the sensitivity can be increased by using synchrotron X-ray (SRXRF), to around 1 part per billion (ppb) for Zn [20]. SRXRF has been applied to quantify multiple heavy metals in different types of biological and environmental samples. Heavy metals like Cr, Mn, Co, Ni and Cu in water samples were quantified by SRXRF, and gave comparable results to the ICP-MS technique [21]. This indicates that SRXRF can be a reliable tool to quantify multi-elements.

The merit of multielemental determination can contribute to the development of novel method for diagnosis or even treatment of diseases [23]. Breast cancer in women is the second most frequent cause of cancer deaths after lung cancer. Trace element concentrations in different human breast tissues (normal, normal adjacent to the tumor, benign and malignant) were analyzed [22]. All trace elements, except Ti, were increased in both malignant and benign tissues while Ca, Cu and Zn were lowered, comparing to normal tissues and normal adjacent tissues. A multivariate discriminant analysis of the observed concentrations of heavy metals was able to successfully identify differences between trace element distributions from normal and malignant tissues with an overall accuracy of 80% and 65% for independent and paired breast samples respectively, and of 87% for benign and malignant tissues.

Prostate cancer is the most frequently diagnosed form of non-cutaneous cancer in men, and the second leading cause of male cancer death in many countries. Analysis of the elemental concentrations (e.g. P, S, K, Ca, Fe, Cu, Zn and Rb) in samples of human prostate tissues with cancer, benign prostate hyperplasia and normal tissues showed a reduction in the concentration of S, K, Ca, Fe, Zn and Rb on the two pathologies studied, compared with the concentrations in normal tissues [24]. These results are comparable to studies using other techniques like NAA and AAS [25,26].

The multielemental determination by SRXRF can contribute to the source apportionment of environmental contaminants. Urban air quality has a strong effect on human health. The most critical

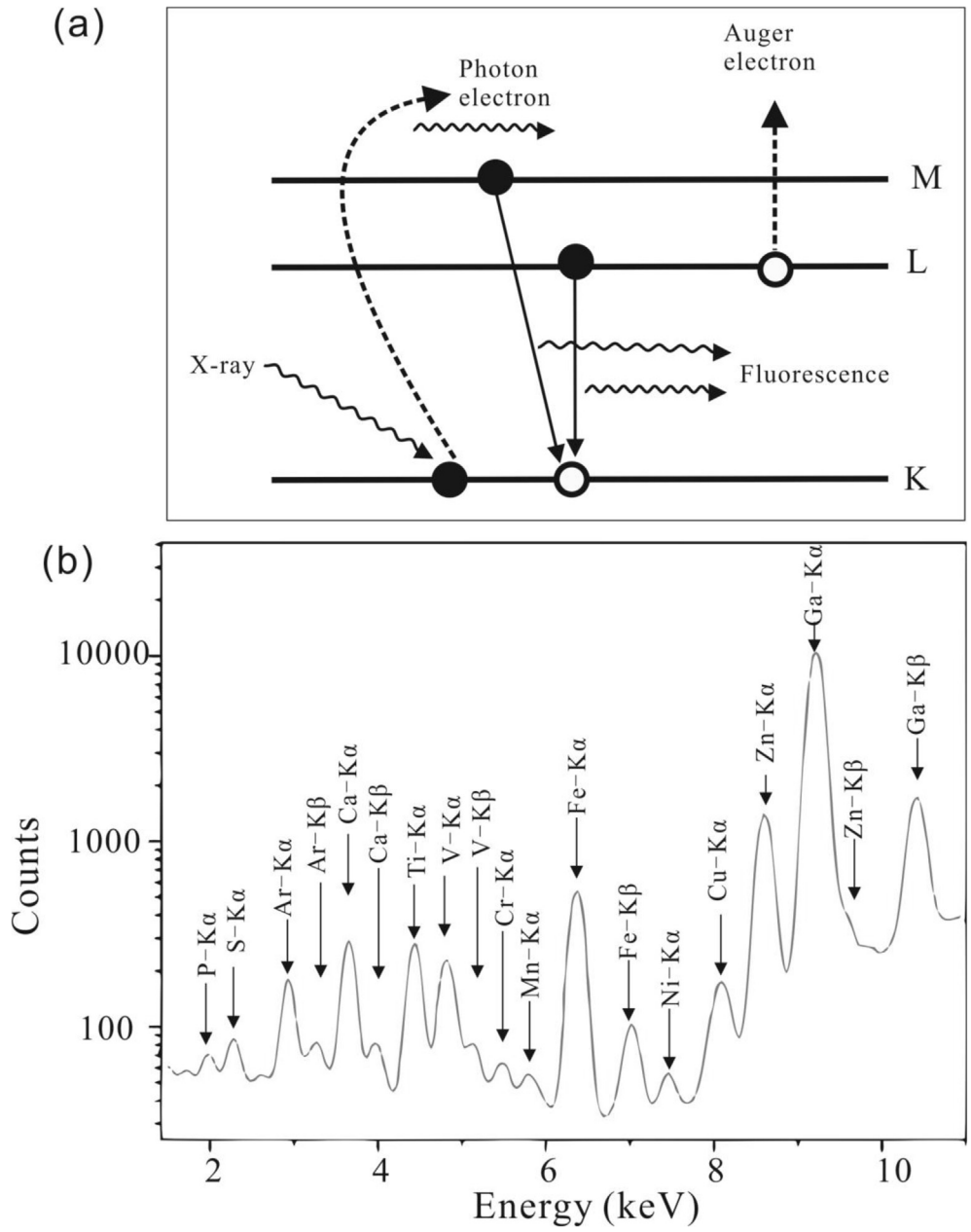

Fig. 1. (a) X-ray fluorescence of the decay of the excited state after X-ray excitation; (b) Typical SRXRF spectrum from a malignant tissue. Reprinted from Ref. [22], Copyright (2009), with permission from Elsevier.

pollutant in atmospheric aerosols is fine particulate matter (PM2.5) (i.e. particles with aerodynamic diameters smaller that 2.5 μm). Strong evidence suggests that PM2.5 causes more severe health effects than particles with larger aerodynamic diameters [27,28]. Besides the size effects, the composition of the particles in aerosols are also an important factor for their adverse health effects [29]. Particles in aerosols were collected according to their aerodynamic diameter through cascade impactors in airports. Trace elements (S, Cl, K, Ca, Ti, Fe, Cu, Zn, Se, Br, Sr, Pb) were analyzed using SRXRF, and typical elements coming from combustion processes (Zn, Pb), aircraft related emissions (Cu), as well as road salting processes (Cl) were detected. This method achieved quantitative determination of ultra-trace amounts (pg/m^3) of elements in the aerosol samples and retained the full size resolution of the impactor, which can correlate the elemental composition of fine particulate matter in different size fractions of aerosols [30].

The multielemental determination by SRXRF together with other techniques can contribute to the new scientific discipline such as Metallomics [4,9,31], which is the study on the metallome in biological system, and Exposomics [32], which is the study of the exposome and relies on other fields such as genomics, metabonomics, lipidomics, transcriptomics and proteomics.

3. Direct speciation of heavy metals

The environmental health effects of heavy metals are not only dependent on the concentration, but also to their chemical forms or species. For example, mercuric selenide (HgSe) has a relatively low toxicity and accumulates as an apparently non-toxic detoxification product in marine animals while dialkylmercury derivatives are extremely toxic, and methylmercury cysteinate was

much less toxic than methylmercury chloride in a zebra fish larvae model system [33].

For the speciation analysis, samples were either digested and then extracted using acid, base, and enzyme or just diluted. The resulting solution was separated by selective techniques like liquid chromatography (LC), gas chromatography (GC), gel electrophoresis (GE) or electro-chromatography (EC). Different species are then monitored by a sensitive and element-specific detector like ICP-MS, and NAA [34,35]. However, this process is time-consuming and the extraction process may destroy or change the chemical species.

Using an intense and energy-tunable source of X-rays, X-ray absorption spectroscopy (XAS) can probe the local geometric and electronic structure surrounding a specific element, which can study the chemical forms or species of heavy metals directly in solid, liquid, or gaseous state [9,36]. This powerful technique can probe the local structure around almost any specific element in the periodic table, which gives information on the number and chemical identities of near neighbors and the average interatomic distances without the requirement for preparation of crystalline samples [14]. Typical X-ray absorption spectra generally have three regions, including the pre-edge, X-ray absorption near-edge structure (XANES), including the first 50–150 eV after the absorption edge and extended X-ray absorption fine structure (EXAFS), which can be detected in suitable samples till 1000 eV and more behind the edge, respectively.

XANES spectra can be used to determine the average oxidation state of the element and the coordination environment of the absorbing atom. By comparing to known references, the chemical form of heavy metals in samples could be identified with little pretreatment. It has been known that MeHg in fish is the primary dietary source for mercury (Hg) in the general public. A comparison of the Hg L_{III} XANES spectrum of swordfish skeletal muscle with the solution spectra of selected standard compounds found that the chemical form of MeHg should be methylmercury cysteinate (MeHgCys), which is less toxic than methylmercury chloride [33]. Rice grown in Hg mining area was found to be another MeHg source for local residents [37,38]. The MeHgCys was also found as the major form of MeHg in rice grain [39,40]. More examples include Se metabolism of the purple bacterium *Rhodobacter sphaeroides*, reduction of As in Indian Mustard, Mn in mitochondria isolated from brain, liver, and heart, Cu and Zn in copper-zinc superoxide dismutase isoforms [41].

EXAFS can also give speciation information by using the oscillations in the EXAFS region. An example is the study on arsenic species and transformation in arsenic hyperaccumulator, Cretan brake (*Pteris cretica L. var ner-vosa* Thunb). It was found that the arsenic in the plant mainly associated with oxygen, while it coordinated with S as As-GSH in root. Most As in plant is present as As(III)-O, indicating that As(V) is reduced to As(III) after it was taken up into the root, and As remained as As(III) when it was transported to the above-ground tissues [42].

Because XAS is a local probe technique, which implies no long range order in sample is required, it can also be applied for quantitative speciation. XANES analysis is based on linear combinations of known spectra from “model compounds”, which is sufficient to estimate ratios of different species.

The direct speciation of Se in Se-enriched yeast was carried out with XANES. By comparison of the XANES spectra of Se-enriched yeast samples with that of the standard Se species, organic R–Se–R (represented by selenomethionine) was found to be the main form. Quantitative speciation through principal component analysis and least-squares linear combination fitting of the Se-enriched yeast samples found 83%, 85% and 81% of R–Se–R selenomethionine for commercial Se-enriched yeast, which is in agreement with the results from HPLC-ICP-MS analysis [31,43].

A main drawback using XAS for speciation is its relatively high detection limit, i.e. the concentration of the element is required to be 10 μg/g or higher [43]. With the introduction of high energy resolution fluorescence detected (HERFD) XAS, the detection limit has been lowered to below μg/g or even a few hundred of ng/g [44,45]. Using HERFD XAS, the source of exposure of Hg in hair samples from seafood, bactericide, dental amalgams or atmosphere was identified, which was supported by molecular modeling [46]. Recently, the Se based selenyl free radicals were distinguished using HERFD XAS through a uniquely low-energy transition with a peak energy at 12 659.0 eV, which corresponds to a 1s → 4p transition to the singly occupied molecular orbital of the free radical [47]. Furthermore, since HERFD XAS has a better spectral resolution than conventional XAS, the precision for the quantitative speciation can also be significantly improved [48]. In all, with the HERFD XAS, it is now possible to study heavy metals in biological samples at realistic concentrations (μg/g or below).

4. Spatial distribution of heavy metals

Besides quantification and speciation of heavy metals in samples, it is also important to know their distribution in the body, which can give information on their trafficking and deposition. Labeling methods like radioactive or stable isotopic tracers or artificial dyes can only give information on the trafficking and distribution of specific metals introduced into the samples [49,50].

The distribution of heavy metals with no introduction of isotopic tracers or artificial dyes can be achieved through mass spectrometry based and X-ray fluorescence based mapping techniques. Mass spectrometry based techniques include laser ablation-ICP-MS (LA-ICP-MS) and microscopic secondary ion mass spectrometry (SIMS). LA-ICP-MS is a powerful tool in the analysis of trace element distribution *in situ* owing to the very high sensitivity of ICP-MS and direct laser sampling capability. LA-ICP-MS has been applied widely for elemental mapping in the environmental samples and biological tissues such as plant leaves, rat brains, human brains and teeth [51–53]. By analyzing secondary ions removed from the sample by sputtering, SIMS can give information on isotopic compositions of small samples with a detection limit of ng/kg level and lateral resolution down to 50 nm, which is called nanoSIMS [54,55]. However, both LA-ICP-MS and SIMS are destructive technique, which may not be a suitable technique for precious samples. Besides, the analysis through SIMS needs high vacuum conditions. On the other hand, the capability of LA-ICP-MS and nanoSIMS for isotope ratio analysis could help to unravel metabolic processes, which is impossible for XRF.

The X-ray fluorescence based mapping techniques includes microscopic EDX (energy dispersive X-ray fluorescence) or WDX (wavelength dispersive x-ray fluorescence), and microscopic proton-induced X-ray emission (PIXE). EDX/WDX coupled to electron microscope can provide very good spatial resolution at about 10 nm, but the detection limit are at about g/kg level which may hold back their application in trace elements detection in biological samples. PIXE has an enhanced sensitivity up to 100 times that of EDX/WDX methods, which can simultaneously detect over 20 elements. It has been applied to elemental distribution in plant and animal tissues [56]. The spatial resolution of 4 μm for PIXE can be achieved by using characteristic Ti-K-X rays (4.558 keV) produced by 3 MeV protons with beam spot size of ~1 μm [57].

However, the mass spectrometry based or X-ray fluorescence based methods are limited by either high detection limits or poor spatial resolution. The synchrotron X-ray fluorescence based

mapping techniques, i.e. SRXRF at the advanced third-generation synchrotron radiation sources, on the other hand, can be effectively used to study heavy metals distribution in small spatial regions (down to 10 nm) with low detection limits (with absolute detection limit below 10^{-17} g) in two- or three-dimension [10,58,59]. A simple comparison between SRXRF and other techniques for spatial distribution analysis of heavy metals is presented in Table 1.

4.1. Two-dimensional mapping

By regulating synchrotron X-rays with a slit or focusing system, such as Kirkpatrick-Baez mirror system, refractive lenses, Fresnel zone plate, and multilayer Laue lens, the beam size can be made into micron or nanometer level while they still have enough photon intensity [59]. Raster scanning of the specimen and acquisition of the entire X-ray spectrum yields quantitative topographical maps for a wide range of elements. Different cells, tissues, and organ slices have successfully been studied using this two-dimensional (2D) SRXRF.

Hg is one of the most hazardous toxic elements while Se is an essential element for animals and human beings [60,61]. Although the antagonistic effect of Hg and Se in animals has been extensively studied, their antagonism in plants remains less explored. SRXRF with micrometer spatial resolution was applied to study the impact of Se on Hg distribution in different tissues of rice plant [62]. It was found that Hg was mainly localized in the epidermis and the pericycle of the rice root. A substantial decrease in Hg accumulation in the epidermis and stele of the rice root can be observed when Se was used. The content of Hg in the leaves collected from the Hg/Se co-exposed rice plant was much less than that of the Hg exposed group, indicating the inhibitive effect of Se on Hg transportation from the roots to the leaves through the vascular cylinder. In rice grain, Hg was principally concentrated on the surface (the aleurone layer), especially along the growth site of the embryo [40]. The concentration of Hg in the embryo part of the rice grain from Se and Hg co-exposed rice was much lower than that of the rice exposed to Hg alone. In addition, SRXRF also showed that the essential elements (Fe, Cu, Zn, K, Ca etc.) were mainly concentrated in the embryo of the rice grain. This suggests that the essential nutrient elements, rather than the toxic elements, can be selectively accumulated in the rice grain. Therefore, SRXRF clearly shows that Se treatment can inhibit Hg uptake and transportation from the rice root to the aerial part, which finally leads to lowered Hg accumulation in the rice grain, especially in the aleuronic layer and embryo. Field studies confirmed that treatment with Se is an efficient way to reduce Hg accumulation (both total Hg and methylmercury) in rice and increase the yield and quality, and subsequently protects the health of the rice-dependent populations in Hg contaminated area [63,64]. In addition, iron plaque and different forms of sulfur were also found to reduce Hg absorption and accumulation in roots and the above-ground parts of rice [65–69].

Hg exposure can affect the distribution of Se in plants. SRXRF mapping showed that Se was mainly concentrated in the stele of the roots, bulbs and the veins of the leaves in garlic (*Allium sativum*), while its accumulation was reduced by Hg. Furthermore, Hg attenuated Se phytotoxicity by reducing uptake of Se by garlic and inhibiting upward transportation of Se from roots [70]. This is also true in rice plant, where there was a negative correlation between Hg and Se in rice grains [71].

SRXRF with beam size reduced to submicrometer level is well-suited for elemental mapping of single cells with subcellular resolution. The subcellular distribution of copper in mouse fibroblast cells was studied with a 200 × 200 nm^2 X-ray beam focused by Fresnel zone plate [72]. The SRXRF confirmed the subcellular localization of Cu in mitochondria and the Golgi apparatus as found by fluorescence microscope. Besides, significant co-localization of Cu and S was found, suggesting that Cu might be primarily coordinated by S-donor ligands.

SRXRF with beam size at nanometer level has been used to study the elemental mapping of Pt-stained human chromosome samples [73]. Ag, Pt, Ba, and Cl were imaged in the chromosome with a single 2D raster mapping. High concentration of Ag, which came from the precursor used in the preparation process of the platinum blue stain, was found. The strong Ba signal corresponds to an unintended contamination while Cl existed at multiple stages of the preparation process. The distribution of Pt is interesting, as it binds to DNA. A large clump of Pt was seen, which results from excessive Pt accumulating along the edge of the sample as the stain evaporates.

The nano SRXRF has also been applied to measure trace element (As, Ca, Cr, Cu, Fe, Mn, Ni, S and Zn) distribution in root epidermis and endodermis during dormancy of *Spartina alterniflora* [74]. The elemental concentrations in the epidermis, outer endodermis and inner endodermis were significantly different. The concentration was higher in the endodermis than that in the epidermis. Furthermore, the elemental concentrations in the outer endodermis were significantly higher than those in the inner endodermis. These results suggest that the Casparian strip may play a role in governing the aplastic transport of these elements.

In addition to imaging the metals in organelles, cells, tissues and organs, 2D SRXRF has been applied to identify the metalloproteins after separation by 2D gel electrophoresis. For example, SRXRF combined with gel filtration chromatography and isoelectric focusing separation has been used to study metalloproteins in human liver cytosol. Two Zn-containing bands, 11 Fe-containing bands and some Cu-containing bands were found [75]. The quantification of metals in metalloproteins was also possible, e.g., Se concentration in a total of 157 seleno-proteins in Se-enriched yeast was found to be 126.56 μg/g, which showed good recovery of Se in the selenoproteins [76].

Table 1
Comparison between SRXRF and selected techniques for spatial distribution analysis of heavy metals.

	Destructive? (Y/N)	Spatial resolution	Isotopic? (Y/N)	Detection limit
Mass spectrometry based				
LA-ICP-MS	Y	μm	Y	ng/kg
SIMS	Y	~50 nm	Y	ng/kg
X-ray based				
EDX/WDX	N	nm	N	g/kg
PIXE	Y	~10 nm	N	10 mg/kg
SRXRF	N	~11 nm	N	μg/kg, ~10^{-17}g (absolute)

4.2. Three-dimensional mapping

Two-dimensional elemental mapping are performed along the sample surface. The information retrieved is a product of the incident X-rays, penetration capability and the self-absorption correction depending on both the energy of the exciting radiation and the energy of the fluorescence radiation, which is not explicitly depth-sensitive. X-rays with sufficient energy can penetrate very deeply (in the order of several hundred microns, even mm range in soft materials) into the samples [77]. Therefore, depth analysis using X-ray can be performed in a non-destructive and non-invasive way, which leads to three-dimensional (3D) mapping. 3D XRF mapping is based either by pencil-shaped primary X-ray beams and reconstruction algorithms similar to the ones used in CT (i.e. SRXRF tomography) [78,79] or using specialized optics on both the X-ray source and detector (confocal XRF) [80,81].

The SRXRF tomography measurement is achieved through measuring a series of projected distributions under various angles and back projected using the appropriate mathematical algorithms [79,82]. Since this method involves rotation of the sample over 180° or 360° relative to the primary beam, it is limited to the investigation of relatively small objects. The spatial resolutions for XRF tomography are situated at the μm level or even less [78,83,84].

SRXRF tomography was used to characterize Fe plaques and related heavy metals on the surface of roots from the aquatic plants *Phalaris arundinacea* (read canarygrass) and *Typha latifolia* (cattail). By using this technique, Pb and Fe was found to accumulate on the surface of the root, forming a covering on the root surface while As was isolated to distinct regions on the exterior and interior of the root [83,85]. Similarly, it was found that As was sequestered by Fe(III) oxyhydroxides within cattail root plaques from a contaminated wetland [86].

The metal compartmentalization and concentration in different tissues of Ni hyperaccumulator *Alyssum murale* was studied using SRXRF tomography [87]. It was found that Ni and Mn concentrated in stem and leaf dermal tissues and in distinct regions associated with the Ca-rich trichomes on the leaf surface. Nickel was concentrated in the xylem and absent from the phloem and cortex in stems while it was isolated in the stele or vascular tissues of the finer root. The opposite pattern was seen for the coarser root, which is devoid of metals on the interior but covered in a “coating” of well-correlated Fe, Zn, and Ni.

The confocal XRF has a depth resolution up to 10 μm and detection limits of sub-mg/kg level. 3D micro-XRF has been successfully applied in biological samples like the root of common duckweed [77], human joint bone [88], and heritage objects like ancient painting, ceramics and Dead Sea Scroll parchment samples [89,90]. One of the obvious advantages for confocal XRF is that the elemental mapping in cross section can be achieved with no necessity to cut the samples into thin slices [77].

The freshwater crustacean *Daphnia magna* is a frequently used ecotoxicological model organism to investigate the mechanisms of toxicity of heavy metals. Dynamic scanning confocal μ-XRF was used to obtain virtual dorsoventral sections of the samples following exposure of *D. magna* to an elevated Zn concentration [91]. Zn was found to be accumulated in the eggs, gut epithelium, ovaries, gills and the carapace of the exposed *D. magna*. Different sub-regions of interest, such as eggs, gut and gill tissues were also analyzed in more detail. Confocal micro-XRF can easily analyze the elemental distribution in different planes of interest. A sagittal section was visualized, enabling it to link specific metal accumulation patterns to corresponding biological/physiological features. For example, different hemoglobin currents inside the organism become confluent at the median dorsal ridge of the carapace before returning to the pericardium around the heart. A more detailed analysis of the ovary located in the front of the gut regarding the reproductive toxicity of dietary Zn exposure was also got.

In general, SRXRF tomography involves long measuring times and challenging data treatment, making it a complex task for 3D determination/visualization of the elemental distributions within a given sample. In contrast, confocal XRF does not require a tomographic reconstruction procedure, and it enables the local analysis of arbitrary sub-volumes inside the sample [91].

5. Spatial speciation of heavy metals

The spatial speciation analysis gives the information on the distribution of different chemical species of heavy metals in the sample.

In the soft X-ray region, scanning transmission X-ray microscopy (STXM) is used in an approach called XANES “stack” imaging, as a stack of repeated 2D scans is acquired. Changing the incident photon energy and taking images with other photon energies gives an image sequence that includes both chemical information and topographical information. Through the third dimension, the XANES spectra can be obtained, and each spatial pixel in the image contains a XANES spectrum and spatially resolved chemical speciation information [92]. This method has been applied to study the spatial speciation distribution of C and Ca in thermally treated lignocellulosic cell walls [93]. It was found that at 500°C the structural integrity of the cell wall was lost and aromatic C═C resonances related to quinones appeared. Besides, it was found that oxalate (CaC_2O_4) was the primary phase of Ca and thermal treatment induced minor Ca phase transition into butschliite ($K_2Ca(CO_3)_2$) and hydroxyapatite ($Ca_5(PO_4)_3OH$).

In the hard X-ray region, the fluorescence signal is often used when acquiring XANES spectra, which will be showcased as follows.

5.1. Two-dimensional speciation

A general scheme for 2D speciation is firstly to study the mapping of the heavy metals by SRXRF, then the speciation of interested element at the “hotspot” is studied using XAS with focused X-ray. *Cardamine enshiensis* is a Se hyperaccumulator plant found in Enshi, a typical seleniferous area in southwestern Hubei province, Central China. The spatial speciation of Se in roots, shoots and leaves of *C. enshiensis* were studied using SRXRF and *in situ* Se K-edge XANES [94]. It was found that Se was primarily located in the cortex, endodermis, and vascular cylinder in roots, while it was in the epidermis, cortex and vascular bundle of shoots and concentrated in the leaf veins and the peripheral parts. *In situ* XANES analysis showed that the root vascular tissue contained 16% SeO_4^{2-}, 19% C-Se^- (using selenocystine, SeCys as model compound) and 65% C-Se-C (using methylselenocystine, MeSeCys as model compound), and shoot vascular bundle contained 10% SeO_4^{2-}, 28% C-Se^- and 62% C-Se-C while leaves had 84% C-Se^- and 16% SeO_3^{2-}(Fig. 2).

However, the above method can only give the speciation information of the interested elements at the selected “hotspot”. On the other hand, by using the tunability of synchrotron radiation, XRF spectra collected at different energies could be used to generate spatial speciation of the interested species [95,96]. The spatial speciation distribution of Se in a hyperaccumulator *Astragalus bisulcatus* (two-grooved poison or milk vetch), a plant capable of accumulating up to 0.65% of its shoot dry biomass as Se in its natural habitat was studied by selectively tuning incident X-ray energies close to the Se K-absorption edge [96]. It was found that plants exposed to selenate for 28 days contained predominantly selenate in the mature leaf tissue, whereas the young leaves and the roots contained organoselenium almost

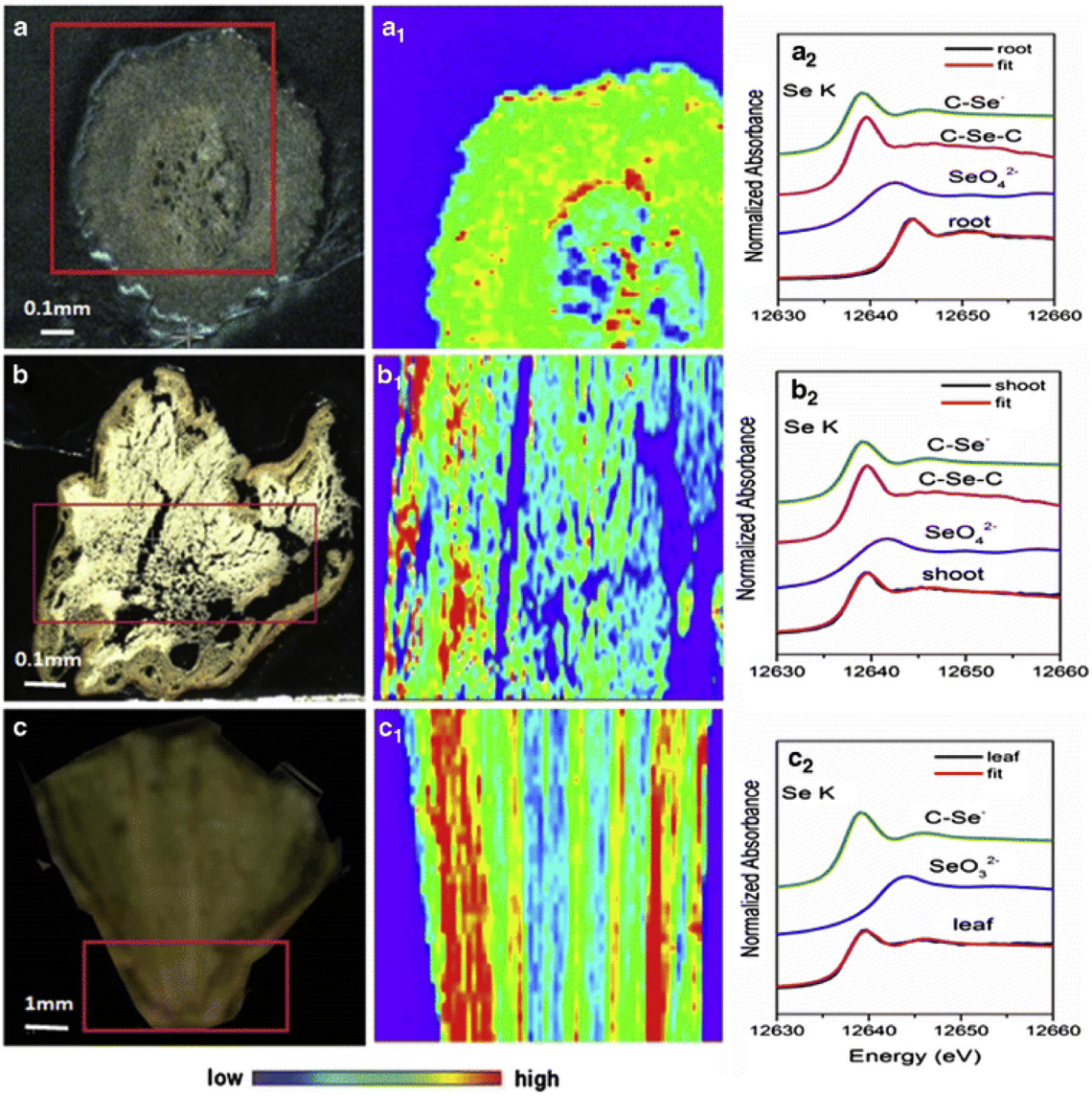

Fig. 2. Optical image, μ-SRXRF mapping of Se and least-square fitting of μ-XANES spectra for roots (cross section, **a**, **a1**, **a2**), shoots (cross section, **b**, **b1**, **b2**) and leaves (**c**, **c1**, **c2**) in *C. enshiensis*. The red boxed area in a, b and c are those for μ-SRXRF mapping in a_1, b_1 and c_1. In a_2, b_2 and c_2, SeO_3^{2-} (selenite), SeO_4^{2-} (selenate), C−Se⁻ (using selenocystine as model compound) and C−Se−C (using methylselenocystine as model compound) were used for least square fitting. Reprinted by permission from Ref. [94]. Copyright (2018) Springer.

exclusively. The concentration of organoselenium in the majority of the root tissue was much lower than that of the youngest leaves, isolated areas on the extremities of the roots contained concentrations of organoselenium of an order of magnitude greater than the rest of the root. This speciation method has also been applied to study Se in the rhizosphere of *Symphyotrichum eatonii* [97].

5.2. Three-dimensional speciation

Just like 3D mapping, 3D speciation could be performed through XRF tomography or confocal XRF.

Stanleya pinnata (prince's plume) is a selenium-hyperaccumulating plant known for its capability to store at least 1000 mg Se kg^{-1} plant dry weight, preferentially accumulating selenate over sulfate [98]. SRXRF tomography has been used to study the speciation of Se in selenite-treated *S. pinnata* stem [99]. The distribution of total Se, inorganic Se(IV) and organic Se was studied and dense Se accumulation was observed close to the vascular bundles in the stems. The reduction of selenite and synthesis of organic selenium in the shoot also occurred.

Full-field XANES employs the full spectra with a large number of incident energies and pixels, which combines the advantages of micro-XANES and micro-XRF [100]. The combination of confocal SRXRF with full-field XANES can be used for speciation [101]. This method was applied to a biochar particle that was reacted with Cr(VI), and it was shown that Cr was primarily distributed near the particle surface. Depth speciation mapping was conducted at 33 representative energies and linear combination fitting (LCF) was performed for the 33 data points from each pixel. It was found that Cr(III) was the primary species with fractions ranging from 0.6 to 1 and the fraction is greater in the interior pixels of the particle than at the surface, while the Cr(VI) fraction is greater at the surface. This method can be applied in a environmental health sciences and other disciplines to delineate depth chemical speciation within intact solid-phase particles.

6. Structure characterization of metal-binding biomolecules

Protein X-ray crystallography (PX) is one of the most powerful tools for the determination of macromolecular 3D structure at a resolution as low as 0.1 nm of metal-binding biomolecules [102]. Crystal structures characterization using synchrotron radiation provide high-resolution snapshots of biomolecules. The higher brightness, flux, and availability of advanced detectors for synchrotron radiation have led to better quality data and higher-resolution crystal structures. A notable example is the characterization of the light atom in nitrogenase, an enzyme that converts nitrogen to ammonia. The 2.2 Å (0.22 nm) resolution structure of nitrogenase detailed an FeMoco with a geometrically complex arrangement of six inner iron atoms and nine surface sulfur atoms [103]. In a later 1.16 Å (0.116 nm) resolution structure, a light atom at the center of the FeMoco was observed but could not be unambiguously assigned [104] while the latest 1.0 Å (0.1 nm) resolution structure clearly identified that the light atom is a carbon atom [105].

Alzheimer's disease (AD) is the main cause of age-related dementia and major brain changes associated with AD pathology include accumulation of amyloid beta (Aβ) protein fragments and formation of extracellular amyloid plaques. Despite numerous structural studies of Cu(II) binding to synthetic Aβ *in vitro*, there is still uncertainty surrounding Cu(II) coordination in Aβ. Using XAS and HERFD XAS, it was found that Cu(II)Aβ(1−42) is sensitive to X-ray photoreduction, changes in buffer composition, peptide concentration, and solution pH [106]. At pH 6.1, only a single histidine residue coordinates Cu(II) in monomeric Aβ(1−42), in addition to 3 other oxygen or nitrogen ligands was observed, while at pH 7.4, the Cu(II) coordination in Aβ(1−42) is similarly 4-coordinate with oxygen and nitrogen ligands.

The three-dimensional structure determinations of biological macromolecules such as proteins and nucleic acids by PX have improved our understanding of many mysteries involved in biological processes. At the same time, these results have clearly confirmed the commonly held belief that H atoms and water molecules around proteins and nucleic acids play a very important role in many physiological functions. However, since it is very hard to identify H atoms accurately in protein molecules by X-ray diffraction alone, a detailed discussion of protonation and hydration sites can only be based upon speculations. In contrast, it is well known that neutron diffraction (NS) provides an experimental method of directly locating H atoms [107]. The combination of NS, PX and XAS can give the structural information including both the locating of H atoms and metal atoms [108,109].

High-throughput (HT) technique of structural characterization using XAS has been achieved. Scott and co-workers designed a 25-well sample holder with 1.5 mm-diameter holes in a 5 × 5 arrangement on a 100 wide polycarbonate holder that fits into a liquid helium-flow XAS cryostat [110]. With the beam apertured to 1 mm × 1 mm, the cryostat and sample holder are rastered first to align the wells, then the metal distribution is determined with a multi-channel energy-discriminating solid-state fluorescence detector. The elemental distribution maps detected by XRF are used to target protein samples for further speciation (by XANES) and structural analysis (by EXAFS) with a 30-element intrinsic germanium detector. This HT XAS method has been used to study the transition metal for 3879 purified proteins from several hundred different protein families [111]. Approximately 9% of the proteins analyzed showed the presence of transition metal atoms (Zn, Cu, Ni, Co, Fe, or Mn) in stoichiometric amounts. Furthermore, by combination of bioinformatics approaches, it can provide comprehensive active site analysis for metalloproteins as a class, revealing new insights into metalloproteins structure and function [111].

It should be noted that properly handling of the samples is vital for structural studies of metal-containing macromolecules, as pH changes, incorporation of unexpected metals, or oxidization/reduction of the metals could cause irreproducibility. Recently, guidelines and best practices for characterizing metal-binding sites in protein structures and alerts experimenters to potential pitfalls during the preparation and handling of metal-containing macromolecules has been developed [112]. By controlling the sample pH, the metal oxidation state using XRF, and collecting diffraction data sets above and below the corresponding metal absorption edges, this protocol allows researchers to gather sufficient evidence to unambiguously determine the identity and location of the metal of interest, as well as to accurately characterize the coordinating ligands in the metal binding domain in the protein.

7. Conclusion and future perspectives

In this review, the state-of-the-art synchrotron-based techniques in quantification, speciation, mapping, and spatial speciation of heavy metals and structure characterization of metal-binding biomolecules in biological samples are reviewed (Fig. 3). SRXRF is a non-destructive, multielemental analytical technique, which has been used in quantification of metals in different biological samples. XAS has been used for speciation of heavy metals while HERFD XAS, can be used to study heavy metals in biological samples at realistic concentrations. The focused synchrotron-based X-ray has been applied to image metals down to nm resolution at 2- or 3- dimension. The combination of XAS with SRXRF can realize 2- or 3- dimension spatial speciation. The structure of metal-binding biomolecules can be characterized by PX and/or XAS, together with NS. Many other synchrotron based techniques like FTIR, XRD and SAXS have been applied in the study of environmental health effects of heavy metals, but was not included in this review [113−117]. It should be pointed out that the beamtime for synchrotron-based techniques is still far from enough and this may hinder the wide application of these techniques. Besides, dedicated tools for data processing are also highly desired.

Future applications of synchrotron based techniques in studies of environmental health effects of heavy metals will require an increase in the capabilities of beamlines. The synchrotron radiation facilities are evolved into low-emittance and quasi-diffraction limit storage rings, either by upgrading the existing facilities (e.g. APS, ESRF, Spring-8, Diamond, ALS, etc.) or by building new ones (such as HEPS in China, SIRIUS in Brazil, MAX IV in Sweden, etc) [45]. The fourth generation light sources, X-ray free electron lasers (FELs), have been built in Europe, Japan, South Korea, USA and China. These new light sources will greatly improve the resolution and sensitivity for the detection of heavy metals in environmental health science [118].

The ability of multimode detection will be an important future capability for synchrotron-based techniques. Presently, if a researcher wishes to use SRXRF to interrogate a region of interest within a sample at substantially higher resolution, it may require a different beamline or a different synchrotron light source. The advantages of being able to dynamically change spatial resolutions on one beamline would be significant [18]. Notably, the simultaneous absorption-, phase- and fluorescence-contrast mapping beamline was constructed at National Synchrotron Light Source (NSLS II), which allows for the observation of the internal ultra-structure of a thick chromosome without sectioning it [59,73].

For the traditional microscope mapping methods, a lens is used to collect the photons scattered by a sample and an image recovered. Although X-ray microscopes with ~10 nm spatial resolution have been demonstrated, ~25 nm is more typical—which is near the wavelength limit [119]. Coherent diffraction imaging (CDI) avoids this limitation by illuminating an object with a laser-like

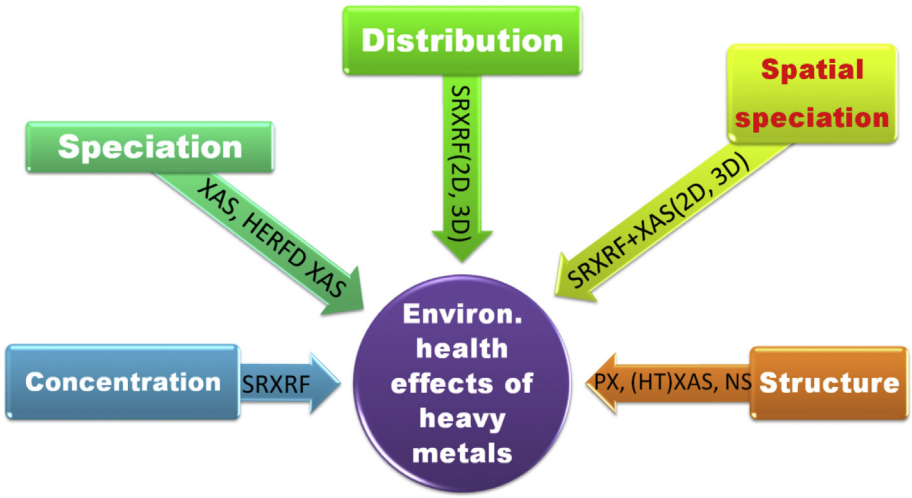

Fig. 3. Synchrotron-based techniques for environmental health effects of heavy metals.

beam and collecting the scattered light on a detector, which is a lensless imaging technique and offers the highest resolution of X-ray images, i.e. 2 and 5.5 nm in the 2D and 3D imaging [120]. CDI has also been extended to speciation analysis using absorption edges, which studied the imaging of Bi at 15 nm resolution in single unstained viruses [121]. This work opened the door for quantitative X-ray imaging of a broad range of specimens from protein machineries and viruses to cellular organelles through CDI. However, it should be pointed out that although CDI is a powerful imaging method with high spatial resolution, it doesn't have strong elements resolution and sensitivity.

Long exposure time to X-ray beam could cause damage to the samples, especially biological samples, which may cause artifacts in both elemental distribution and chemical speciation. It is therefore essential to preserve the sample using cryogenic conditions or preferably through reducing the radiation dose by using fast detector technologies [122]. This can drastically reduce the exposure duration and radiation doses [92].

The improved speed of data acquisition and sample scanning systems have increased the amount of raw data collected during each experiment. With the huge increase in data volume, the current lack of automated data analysis pipelines prevents the fine-tuning of beam-time experiments. Besides, the lack of appropriate data analysis environment limits the realization of experiments that generate a large amount of data in a very short period of time. To address these problems, a big data strategies is proposed, which can increase the number of scientific discoveries [123].

Acknowledgements

We thank Professor Herman Autrup for his critical reading and constructive comments. We thank the financial support from National Natural Science Foundation of China (11975247; 11475196; 41877405), Ministry of Science and Technology of China (2016YFA0201600), and Guizhou Department of Science and Technology (No. QKH-2016-2804). We gratefully acknowledge the staff from Beijing Synchrotron Radiation Facility, Shanghai Synchrotron Radiation Facility and National Synchrotron Radiation Laboratory for beam time allocation and assistance during data collection.

References

[1] X. Guo, Environmental Health Science, Peking University Medical Press, Beijing, 2006.
[2] Q. Wang, W.-J. Zhang, L.-Y. He, X.-F. Sheng, Increased biomass and quality and reduced heavy metal accumulation of edible tissues of vegetables in the presence of Cd-tolerant and immobilizing *Bacillus megaterium* H3, Ecotoxicol. Environ. Saf. 148 (2018) 269–274.
[3] H. Etesami, Bacterial mediated alleviation of heavy metal stress and decreased accumulation of metals in plant tissues: mechanisms and future prospects, Ecotoxicol. Environ. Saf. 147 (2018) 175–191.
[4] Y.-F. Li, H. Sun, C. Chen, Z. Chai, Metallomics, Science Press, Beijing, 2016.
[5] L. Hu, B. He, Y. Wang, G. Jiang, H. Sun, Metallomics in environmental and health related research: current status and perspectives, Chin. Sci. Bull. 58 (2) (2013) 169–176.
[6] P. Grandjean, P.J. Landrigan, Developmental neurotoxicity of industrial chemicals, Lancet 368 (9553) (2006) 2167–2178.
[7] J. Szpunar, Metallomics: a new frontier in analytical chemistry, Anal. Bioanal. Chem. 378 (1) (2004) 54–56.
[8] Y.-F. Li, Y. Gao, C. Chen, B. Li, Y. Zhao, Z. Chai, High throughput analytical techniques in metallomics and the perspectives, Sci. Sin. Chim. 39 (2) (2009) 1–10.
[9] C. Chen, Z. Chai, Y. Gao, Nuclear Analytical Techniques for Metallomics and Metalloproteomics, RSC publishing, Cambridge, 2010.
[10] L. Wang, L. Yan, J. Liu, C. Chen, Y. Zhao, Quantification of nanomaterial/nanomedicine trafficking in vivo, Anal. Chem. 90 (1) (2018) 589–614.
[11] L. Luo, S. Zhang, Applications of synchrotron-based X-ray techniques in environmental science, Sci. China Chem. 53 (12) (2010) 2529–2538.
[12] Y.-F. Li, J. Zhao, Y. Li, X. Xu, L. Cui, B. Zhang, S. Shan, Y. Geng, J. Li, B. Li, Y. Gao, Studies on the environmental health effects and ecotoxicology of mercury by synchrotron radiation-based techniques, Sci. Sin. Chim. 45 (1) (2015) 1–17.
[13] Y.-F. Li, J. Zhao, Y. Qu, Y. Gao, Z. Guo, Z. Liu, Y. Zhao, C. Chen, Synchrotron radiation techniques for nanotoxicology, Nanomed. Nanotechnol. Biol. Med. 11 (2015) 1531–1549.
[14] Z. Mai, Synchrotron Radiation Light Source and its Application, Science Press, Beijing, 2013.
[15] G.E. Brown, V.E. Henrich, W.H. Casey, D.L. Clark, C. Eggleston, A. Felmy, D.W. Goodman, M. Grätzel, G. Maciel, M.I. McCarthy, K.H. Nealson, D.A. Sverjensky, M.F. Toney, J.M. Zachara, Metal oxide surfaces and their interactions with aqueous solutions and microbial organisms, Chem. Rev. 99 (1) (1999) 77–174.
[16] D.L. Sparks, in: J. Xu, P.M. Huang (Editors), In Advances in the Use of Synchrotron Radiation to Elucidate Environmental Interfacial Reaction Processes and Mechanisms in the Earth's Critical Zone, Berlin, Heidelberg, 2010, Springer Berlin Heidelberg, Berlin, Heidelberg, 2010, pp. 3–4.
[17] W.-Q. Shi, L.-Y. Yuan, C.-Z. Wang, L. Wang, L. Mei, C.-L. Xiao, L. Zhang, Z.-J. Li, Y.-L. Zhao, Z.-F. Chai, Exploring actinide materials through synchrotron radiation techniques, Adv. Mater. 26 (46) (2014) 7807–7848.
[18] M.J. Pushie, I.J. Pickering, M. Korbas, M.J. Hackett, G.N. George, Elemental and chemically specific X-ray fluorescence imaging of biological systems, Chem. Rev. 114 (17) (2014) 8499–8541.
[19] J. Szpunar, Advances in analytical methodology for bioinorganic speciation analysis: metallomics, metalloproteomics and heteroatom-tagged proteomics and metabolomics, Analyst 130 (4) (2005) 442–465.
[20] A. Ji, Development of X-ray fluorescence spectrometry in the 30 Years, Rock Miner. Anal. 31 (3) (2012) 383–398.
[21] L.L. Wang, H.S. Yu, L.N. Li, X.J. Wei, Y.Y. Huang, The development of TXRF method and its application on the study of trace elements in water at SSRF, Nucl. Instrum. Methods Phys. Res. B 375 (2016) 49–55.
[22] M. Piacenti da Silva, O.L.A.D. Zucchi, A. Ribeiro-Silva, M.E. Poletti, Discriminant analysis of trace elements in normal, benign and malignant breast

tissues measured by total reflection X-ray fluorescence, Spectrochim. Acta B 64 (6) (2009) 587–592.
[23] B. Callejón-Leblic, J.L. Gómez-Ariza, A. Pereira-Vega, T. García-Barrera, Metal dyshomeostasis based biomarkers of lung cancer using human biofluids, Metallomics 10 (10) (2018) 1444–1451.
[24] R.G. Leitão, A. Palumbo, P.A.V.R. Souza, G.R. Pereira, C.G.L. Canellas, M.J. Anjos, L.E. Nasciutti, R.T. Lopes, Elemental concentration analysis in prostate tissues using total reflection X-ray fluorescence, Radiat. Phys. Chem. 95 (2014) 62–64.
[25] V. Zaichick, INAA and EDXRF applications in the age dynamics assessment of Zn content and distribution in the normal human prostate, J. Radioanal. Nucl. Chem. 262 (1) (2004) 229–234.
[26] M. Yaman, D. Atici, S. Bakırdere, İ. Akdeniz, Comparison of trace metal concentrations in malign and benign human prostate, J. Med. Chem. 48 (2) (2005) 630–634.
[27] M. Mei, H. Song, L. Chen, B. Hu, R. Bai, D. Xu, Y. Liu, Y. Zhao, C. Chen, Early-life exposure to three size-fractionated ultrafine and fine atmospheric particulates in Beijing exacerbates asthma development in mature mice, Part. Fibre Toxicol. 15 (1) (2018) 13.
[28] J. Ding, J. Guo, L. Wang, Y. Chen, B. Hu, Y. Li, R. Huang, J. Cao, Y. Zhao, M. Geiser, Q. Miao, Y. Liu, C. Chen, Cellular responses to exposure to outdoor air from the Chinese Spring Festival at the air–liquid interface, Environ. Sci. Technol. 53 (15) (2019) 9128–9138.
[29] H. Jing, Y.-F. Li, J. Zhao, B. Li, J. Sun, R. Chen, Y. Gao, C. Chen, Wide-range particle characterization and elemental concentration in Beijing aerosol during the 2013 Spring Festival, Environ. Pollut. 192 (2014) 204–211.
[30] V. Groma, J. Osan, A. Alsecz, S. Torok, F. Meirer, C. Streli, P. Wobrauschek, G. Falkenberg, Trace element analysis of airport related aerosols using SR-TXRF, Q. J. Hung Meteorol. Service 112 (2) (2008) 83–97.
[31] S. Mounicou, J. Szpunar, R. Lobinski, Metallomics: the concept and methodology, Chem. Soc. Rev. 38 (4) (2009) 1119–1138.
[32] Y. Cui, D.M. Balshaw, R.K. Kwok, C.L. Thompson, G.W. Collman, L.S. Birnbaum, The Exposome: embracing the complexity for discovery in environmental health, Environ. Health Perspect. 124 (8) (2016) A137–A140.
[33] H.H. Harris, I.J. Pickering, G.N. George, The chemical form of mercury in fish, Science 301 (5637) (2003), 1203–1203.
[34] Z. Chai, X. Mao, Z. Hu, Z. Zhang, C. Chen, W. Feng, S. Hu, H. Ouyang, Overview of the methodology of nuclear analytical techniques for speciation studies of trace elements in the biological and environmental sciences, Anal. Bioanal. Chem. 372 (3) (2002) 407–411.
[35] Y.-F. Li, C. Chen, B. Li, Q. Wang, J. Wang, Y. Gao, Y. Zhao, Z. Chai, Simultaneous speciation of selenium and mercury in human urine samples from long-term mercury-exposed populations with supplementation of selenium-enriched yeast by HPLC-ICP-MS, J. Anal. At. Spectrom. 22 (8) (2007) 925–930.
[36] Y.-F. Li, C. Chen, B. Li, W. Li, L. Qu, Z. Dong, M. Nomura, Y. Gao, J. Zhao, W. Hu, Y. Zhao, Z. Chai, Mercury in human hair and blood samples from people living in Wanshan mercury mine area, Guizhou, China: an XAS study, J. Inorg. Biochem. 102 (3) (2008) 500–506.
[37] P. Li, X. Feng, G. Qiu, Methylmercury exposure and health effects from rice and fish consumption: a review, Int. J. Environ. Res. Public Health 7 (6) (2010) 2666–2691.
[38] X. Feng, P. Li, G. Qiu, S. Wang, G. Li, L. Shang, B. Meng, H. Jiang, W. Bai, Z. Li, X. Fu, Human exposure to methylmercury through rice intake in mercury mining areas, Guizhou province, China, Environ. Sci. Technol. 42 (1) (2008) 326–332.
[39] L. Li, F. Wang, B. Meng, M. Lemes, X. Feng, G. Jiang, Speciation of methylmercury in rice grown from a mercury mining area, Environ. Pollut. 158 (10) (2010) 3103–3107.
[40] B. Meng, X. Feng, G. Qiu, C.W.N. Anderson, J. Wang, L. Zhao, Localization and speciation of mercury in brown rice with implications for Pan-Asian public health, Environ. Sci. Technol. 48 (14) (2014) 7974–7981.
[41] S. Chevreux, S. Roudeau, A. Fraysse, A. Carmona, G. Devès, P.L. Solari, T.C. Weng, R. Ortega, Direct speciation of metals in copper-zinc superoxide dismutase isoforms on electrophoresis gels using X-ray absorption near edge structure, J. Anal. At. Spectrom. 23 (8) (2008) 1117–1120.
[42] Z. Huang, T. Chen, M. Lei, T. Hu, Q. Huang, EXAFS study on arsenic species and transformation in arsenic hyperaccumulator, Sci. China Chem. C Life Sci. 47 (2) (2004) 124–129.
[43] Y.-F. Li, X. Wang, L. Wang, B. Li, Y. Gao, C. Chen, Direct quantitative speciation of selenium in selenium-enriched yeast and yeast-based products by X-ray absorption spectroscopy confirmed by HPLC-ICP-MS, J. Anal. At. Spectrom. 25 (3) (2010) 426–430.
[44] M. Bauer, HERFD-XAS and valence-to-core-XES: new tools to push the limits in research with hard X-rays? Phys. Chem. Chem. Phys. 16 (27) (2014) 13827–13837.
[45] W. Xu, Z. Du, S. Liu, Y. Zhu, C. Xiao, A. Marcelli, Perspectives of XRF and XANES applications in cryospheric sciences using Chinese SR facilities, Cond. Matter. 3 (4) (2018) 29.
[46] A. Manceau, M. Enescu, A. Simionovici, M. Lanson, M. Gonzalez-Rey, M. Rovezzi, R. Tucoulou, P. Glatzel, K.L. Nagy, J.-P. Bourdineaud, Chemical forms of mercury in human hair reveal sources of exposure, Environ. Sci. Technol. 50 (19) (2016) 10721–10729.
[47] S. Nehzati, N.V. Dolgova, D. Sokaras, T. Kroll, J.J.H. Cotelesage, I.J. Pickering, G.N. George, A photochemically generated selenyl free radical observed by high energy resolution fluorescence detected X-ray absorption spectroscopy, Inorg. Chem. 57 (17) (2018) 10867–10872.
[48] O. Proux, E. Lahera, W. Del Net, I. Kieffer, M. Rovezzi, D. Testemale, M. Irar, S. Thomas, A. Aguilar-Tapia, E.F. Bazarkina, A. Prat, M. Tella, M. Auffan, J. Rose, J.-L. Hazemann, High-energy resolution fluorescence detected X-Ray absorption spectroscopy: a powerful new structural tool in environmental biogeochemistry sciences, J. Environ. Qual. 46 (6) (2017) 1146–1157.
[49] M.T. Zhu, W.Y. Feng, Y. Wang, B. Wang, M. Wang, H. Ouyang, Y.L. Zhao, Z.F. Chai, Particokinetics and extrapulmonary translocation of intratracheally instilled ferric oxide nanoparticles in rats and the potential health risk assessment, Toxicol. Sci. 107 (2) (2009) 342–351.
[50] K.J. Lee, P.D. Nallathamby, L.M. Browning, C.J. Osgood, X.-H.N. Xu, *In vivo* imaging of transport and biocompatibility of single silver nanoparticles in early development of zebrafish embryos, ACS Nano 1 (2) (2007) 133–143.
[51] B. Jackson, S. Harper, L. Smith, J. Flinn, Elemental mapping and quantitative analysis of Cu, Zn, and Fe in rat brain sections by laser ablation ICP-MS, Anal. Bioanal. Chem. 384 (4) (2006) 951–957.
[52] J.S. Becker, M. Zoriy, M. Przybylski, J.S. Becker, High resolution mass spectrometric brain proteomics by MALDI-FTICR-MS combined with determination of P, S, Cu, Zn and Fe by LA-ICP-MS, Int. J. Mass Spectrom. 261 (1) (2007) 68–73.
[53] D. Kang, D. Amarasiriwardena, A. Goodman, Application of laser ablation–inductively coupled plasma-mass spectrometry (LA–ICP–MS) to investigate trace metal spatial distributions in human tooth enamel and dentine growth layers and pulp, Anal. Bioanal. Chem. 378 (6) (2004) 1608–1615.
[54] K.L. Moore, E. Lombi, F.-J. Zhao, C.R.M. Grovenor, Elemental imaging at the nanoscale: NanoSIMS and complementary techniques for element localisation in plants, Anal. Bioanal. Chem. 402 (10) (2012) 3263–3273.
[55] D. Schaumlöffel, R. Hutchinson, J. Malherbe, P.L. Coustumer, E. Gontier, M.P. Isaure, Novel methods for bioimaging including LA-ICP-MS, NanoSIMS, TEM/X-EDS, and SXRF, in: B. Michalke (Editor), Metallomics: Analytical Techniques and Speciation Methods, Wiley-VCH, Weinheim, 2016, pp. 83–116.
[56] G. Tylko, J. Mesjasz-Przybylowicz, W.J. Przybylowicz, In-vacuum micro-PIXE analysis of biological specimens in frozen-hydrated state, Nucl. Instrum. Methods Phys. Res. B 260 (1) (2007) 141–148.
[57] K. Ishii, S. Matsuyama, Y. Watanabe, Y. Kawamura, T. Yamaguchi, R. Oyama, G. Momose, A. Ishizaki, H. Yamazaki, Y. Kikuchi, 3D-imaging using micro-PIXE, Nucl. Instrum. Methods Phys. Res. 571 (1–2) (2007) 64–68.
[58] C. Schroer, O. Kurapova, J. Patommel, P. Boye, J. Feldkamp, B. Lengeler, M. Burghammer, C. Riekel, L. Vincze, A. Van der Hart, Hard x-ray nanoprobe based on refractive X-ray lenses, Appl. Phys. Lett. 87 (2005) 124103.
[59] H. Yan, N. Bouet, J. Zhou, X. Huang, E. Nazaretski, W. Xu, A.P. Cocco, W.K.S. Chiu, K.S. Brinkman, Y.S. Chu, Multimodal hard x-ray imaging with resolution approaching 10 nm for studies in material science, Nano Futures 2 (1) (2018) 011001.
[60] Y.-F. Li, L. Shang, J. Zhao, H. Hu, W. Wang, Environmental Bioinorganic Chemistry of Mercury, Science Press, Beijing, 2018, p. 329.
[61] P. Li, S. Guo, J. Zhao, Y. Gao, Y.-F. Li, Human biological monitoring of mercury through hair samples in China, Bull. Environ. Contam. Toxicol. 102 (5) (2019) 701–707.
[62] J. Zhao, Y.-F. Li, Y. Li, Y. Gao, B. Li, Y. Hu, Y. Zhao, Z. Chai, Selenium modulates mercury uptake and distribution in rice (*Oryza sativa* L.), in correlation to mercury species and exposure level, Metallomics 6 (10) (2014) 1951–1957.
[63] Y.-F. Li, J. Zhao, Y. Li, H. Li, J. Zhang, B. Li, Y. Gao, C. Chen, M. Luo, R. Huang, J. Li, The concentration of selenium matters: a field study on mercury accumulation in rice by selenite treatment in Qingzhen, Guizhou, China, Plant Soil 391 (1–2) (2015) 195–205.
[64] Y. Li, W. Hu, J. Zhao, Q. Chen, W. Wang, B. Li, Y.-F. Li, Selenium decreases methylmercury and increases nutritional elements in rice growing in mercury-contaminated farmland, Ecotoxicol. Environ. Saf. 182 (2019) 109447.
[65] Y. Li, J. Zhao, H. Zhong, Y. Wang, H. Li, Y.-F. Li, V. Liem-Nguyen, T. Jiang, Z. Zhang, Y. Gao, Z. Chai, Understanding enhanced microbial MeHg production in mining-contaminated paddy soils under sulfate amendment: changes in Hg mobility or microbial methylators? Environ. Sci. Technol. 53 (4) (2019) 1844–1852.
[66] Y. Li, J. Zhao, J. Guo, M. Liu, Q. Xu, H. Li, Y.-F. Li, L. Zheng, Z. Zhang, Y. Gao, Influence of sulfur on the accumulation of mercury in rice plant (*Oryza sativa* L.) growing in mercury contaminated soils, Chemosphere 182 (2017) 293–300.
[67] Y. Li, J. Zhao, B. Zhang, Y. Liu, X. Xu, Y.-F. Li, B. Li, Y. Gao, Z. Chai, The influence of iron plaque on the absorption, translocation and transformation of mercury in rice (*Oryza sativa* L.) seedlings exposed to different mercury species, Plant Soil 398 (1) (2016) 87–97.
[68] Y. Li, H. Li, Y. Yu, J. Zhao, Y. Wang, C. Hu, H. Li, G. Wang, Y. Li, Y. Gao, Thiosulfate amendment reduces mercury accumulation in rice (*Oryza sativa* L.), Plant Soil 430 (1) (2018) 413–422.
[69] X. Bai, Y. Li, X. Liang, H. Li, J. Zhao, Y.-F. Li, Y. Gao, Botanic metallomics of mercury and selenium: current understanding of mercury-selenium antagonism in plant with the traditional and advanced technology, Bull. Environ. Contam. Toxicol. 102 (5) (2019) 628–634.

[70] J. Zhao, Y. Hu, Y. Gao, Y. Li, B. Li, Y. Dong, Z. Chai, Mercury modulates selenium activity via altering its accumulation and speciation in garlic (*Allium sativum*), Metallomics 5 (7) (2013) 896–903.

[71] C. Zhang, G. Qiu, C.W.N. Anderson, H. Zhang, B. Meng, L. Liang, X. Feng, Effect of atmospheric mercury deposition on selenium Accumulation in rice (*Oryza sativa* L.) at a mercury mining region in Southwestern China, Environ. Sci. Technol. 49 (6) (2015) 3540–3547.

[72] L. Yang, R. McRae, M.M. Henary, R. Patel, B. Lai, S. Vogt, C.J. Fahrni, Imaging of the intracellular topography of copper with a fluorescent sensor and by synchrotron X-ray fluorescence microscopy, Proc. Natl. Acad. Sci. U.S.A. 102 (32) (2005) 11179–11184.

[73] H. Yan, E. Nazaretski, K. Lauer, X. Huang, U. Wagner, C. Rau, M. Yusuf, I. Robinson, S. Kalbfleisch, L. Li, N. Bouet, J. Zhou, R. Conley, Y.S. Chu, Multimodality hard-x-ray imaging of a chromosome with nanoscale spatial resolution, Sci. Rep. 6 (2016) 20112.

[74] H. Feng, Y. Qian, J.K. Cochran, Q. Zhu, W. Hu, H. Yan, L. Li, X. Huang, Y.S. Chu, H. Liu, S. Yoo, C.-J. Liu, Nanoscale measurement of trace element distributions in *Spartina alterniflora* root tissue during dormancy, Sci. Rep. 7 (2017) 40420.

[75] Y. Gao, Y. Liu, C. Chen, B. Li, W. He, Y. Huang, Z. Chai, Combination of synchrotron radiation X-ray fluorescence with isoelectric focusing for study of metalloprotein distribution in cytosol of hepatocellular carcinoma and surrounding normal tissues, J. Anal. At. Spectrom. 20 (5) (2005) 473–475.

[76] J. Zhao, Y. Pu, Y. Gao, X. Peng, Y. Li, X. Xu, B. Li, N. Zhu, J. Dong, G. Wu, Y.-F. Li, Identification and quantification of seleno-proteins by 2-DE-SR-XRF in selenium-enriched yeasts, J. Anal. At. Spectrom. 30 (2015) 1408–1413.

[77] B. Kanngießer, W. Malzer, M. Pagels, L. Lühl, G. Weseloh, Three-dimensional micro-XRF under cryogenic conditions: a pilot experiment for spatially resolved trace analysis in biological specimens, Anal. Bioanal. Chem. 389 (4) (2007) 1171–1176.

[78] P. Bleuet, P. Gergaud, L. Lemelle, P. Bleuet, R. Tucoulou, P. Cloetens, J. Susini, G. Delette, A. Simionovici, 3D chemical imaging based on a third-generation synchrotron source, TrAC Trends Anal. Chem. 29 (6) (2010) 518–527.

[79] H. Gan, H. Gao, H. Zhu, J. Chen, P. Zhu, D. Xian, X-ray fluorescence tomography, Laser Optoelectr. Prog. 43 (3) (2006) 56–64.

[80] L. Vincze, B. Vekemans, F.E. Brenker, G. Falkenberg, K. Rickers, A. Somogyi, M. Kersten, F. Adams, Three-dimensional trace element analysis by confocal X-ray microfluorescence imaging, Anal. Chem. 76 (22) (2004) 6786–6791.

[81] B. Kanngießer, W. Malzer, I. Reiche, A new 3D micro X-ray fluorescence analysis set-up - first archaeometric applications, Nucl. Instrum. Methods Phys. Res. B 211 (2) (2003) 259–264.

[82] L. Vincze, B. Vekemans, I. Szaloki, K. Janssens, R. Van Grieken, H. Feng, K.W. Jones, F. Adams, in: U. Bonse Ulrich (Editor), In High Resolution X-Ray Fluorescence Micro-tomography on Single Sediment Particles, 46th SPIE Annual Meeting International Symposium of Optical Science and Technology, San Diego, 2001, pp. 240–245. San Diego.

[83] C.M. Hansel, M.J. La Force, S. Fendorf, S. Sutton, Spatial and temporal association of As and Fe species on aquatic plant roots, Environ. Sci. Technol. 36 (9) (2002) 1988–1994.

[84] B. Laforce, B. Masschaele, M.N. Boone, D. Schaubroeck, M. Dierick, B. Vekemans, C. Walgraeve, C. Janssen, V. Cnudde, L. Van Hoorebeke, L. Vincze, Integrated three-dimensional microanalysis combining X-ray microtomography and X-ray fluorescence methodologies, Anal. Chem. 89 (19) (2017) 10617–10624.

[85] C.M. Hansel, S. Fendorf, S. Sutton, M. Newville, Characterization of Fe plaque and associated metals on the roots of mine-waste impacted aquatic plants, Environ. Sci. Technol. 35 (19) (2001) 3863–3868.

[86] N.K. Blute, D.J. Brabander, H.F. Hemond, S.R. Sutton, M.G. Newville, M.L. Rivers, Arsenic sequestration by ferric iron plaque on Cattail toots, Environ. Sci. Technol. 38 (22) (2004) 6074–6077.

[87] D.H. McNear, E. Peltier, J. Everhart, R.L. Chaney, S. Sutton, M. Newville, M. Rivers, D.L. Sparks, Application of quantitative fluorescence and absorption-edge computed microtomography to image metal compartmentalization in *Alyssum murale*, Environ. Sci. Technol. 39 (7) (2005) 2210–2218.

[88] N. Zoeger, C. Streli, P. Wobrauschek, C. Jokubonis, G. Pepponi, P. Roschger, J. Hofstaetter, A. Berzlanovich, D. Wegrzynek, E. Chinea-Cano, A. Markowicz, R. Simon, G. Falkenberg, Determination of the elemental distribution in human joint bones by SR micro XRF, X-Ray Spectrom 37 (1) (2008) 3–11.

[89] L. Yi, M. Qin, K. Wang, X. Lin, S. Peng, T. Sun, Z. Liu, The three-dimensional elemental distribution based on the surface topography by confocal 3D-XRF analysis, Appl. Phys. A 122 (9) (2016) 856.

[90] I. Mantouvalou, T. Wolff, O. Hahn, I. Rabin, L. Lühl, M. Pagels, W. Malzer, B. Kanngiesser, 3D Micro-XRF for cultural heritage objects: new analysis strategies for the investigation of the Dead Sea scrolls, Anal. Chem. 83 (16) (2011) 6308–6315.

[91] B. De Samber, G. Silversmit, K. De Schamphelaere, R. Evens, T. Schoonjans, B. Vekemans, C. Janssen, B. Masschaele, L. Van Hoorebeke, I. Szalóki, F. Vanhaecke, K. Rickers, G. Falkenberg, L. Vincze, Element-to-tissue correlation in biological samples determined by three-dimensional X-ray imaging methods, J. Anal. At. Spectrom. 25 (4) (2010) 544–553.

[92] E. Lombi, M.D. de Jonge, E. Donner, C.G. Ryan, D. Paterson, Trends in hard X-ray fluorescence mapping: environmental applications in the age of fast detectors, Anal. Bioanal. Chem. 400 (6) (2011) 1637–1644.

[93] M. Thyrel, R. Backman, K. Thånell, C. Karunakaran, U. Skyllberg, T.A. Lestander, Nanomapping and speciation of C and Ca in thermally treated lignocellulosic cell walls using scanning transmission X-ray microscopy and K-edge XANES, Fuel 167 (2016) 149–157.

[94] L. Cui, J. Zhao, J. Chen, W. Zhang, Y. Gao, B. Li, Y.-F. Li, Translocation and transformation of selenium in hyperaccumulator plant *Cardamine enshiensis* from Enshi, Hubei, China, Plant Soil 425 (1–2) (2018) 577–588.

[95] I.J. Pickering, L. Gumaelius, H.H. Harris, R.C. Prince, G. Hirsch, J.A. Banks, D.E. Salt, G.N. George, Localizing the biochemical transformations of arsenate in a hyperaccumulating fern, Environ. Sci. Technol. 40 (16) (2006) 5010–5014.

[96] I.J. Pickering, R.C. Prince, D.E. Salt, G.N. George, Quantitative, chemically specific imaging of selenium transformation in plants, Proc. Natl. Acad. Sci. U.S.A. 97 (20) (2000) 10717–10722.

[97] L.L. Oram, D.G. Strawn, G. Möller, Chemical speciation and bioavailability of selenium in the rhizosphere of *Symphyotrichum eatonii* from reclaimed mine soils, Environ. Sci. Technol. 45 (3) (2011) 870–875.

[98] J.L. Freeman, L.H. Zhang, M.A. Marcus, S. Fakra, S.P. McGrath, E.A.H. Pilon-Smits, Spatial imaging, speciation, and quantification of selenium in the hyperaccumulator plants *Astragalus bisulcatus* and *Stanleya pinnata*, Plant Physiol. 142 (1) (2006) 124–134.

[99] W. Amos, S. Webb, Y. Liu, J.C. Andrews, D.L. LeDuc, Imaging translocation and transformation of bioavailable selenium by *Stanleya pinnata* with X-ray microscopy, Anal. Bioanal. Chem. 404 (5) (2012) 1277–1285.

[100] B. Hesse, M. Salome, H. Castillo-Michel, M. Cotte, B. Fayard, C.J. Sahle, W. De Nolf, J. Hradilova, A. Masic, B. Kanngießer, M. Bohner, P. Varga, K. Raum, S. Schrof, Full-field calcium K-Edge X-ray absorption near-edge structure spectroscopy on cortical bone at the micron-scale: polarization effects reveal mineral orientation, Anal. Chem. 88 (7) (2016) 3826–3835.

[101] P. Liu, C.J. Ptacek, D.W. Blowes, Y.Z. Finfrock, M. Steinepreis, F. Budimir, A method for redox mapping by confocal micro-X-ray fluorescence imaging: using chromium species in a biochar particle as an example, Anal. Chem. 91 (8) (2019) 5142–5149.

[102] S.E.J. Bowman, J. Bridwell-Rabb, C.L. Drennan, Metalloprotein crystallography: more than a structure, Acc. Chem. Res. 49 (4) (2016) 695–702.

[103] J. Kim, D. Rees, Structural models for the metal centers in the nitrogenase molybdenum-iron protein, Science 257 (5077) (1992) 1677–1682.

[104] O. Einsle, F.A. Tezcan, S.L.A. Andrade, B. Schmid, M. Yoshida, J.B. Howard, D.C. Rees, Nitrogenase MoFe-Protein at 1.16 Å resolution: a central ligand in the FeMo-cofactor, Science 297 (5587) (2002) 1696–1700.

[105] T. Spatzal, M. Aksoyoglu, L. Zhang, S.L.A. Andrade, E. Schleicher, S. Weber, D.C. Rees, O. Einsle, Evidence for interstitial carbon in nitrogenase FeMo cofactor, Science 334 (6058) (2011), 940–940.

[106] K.L. Summers, K.M. Schilling, G. Roseman, K.A. Markham, N.V. Dolgova, T. Kroll, D. Sokaras, G.L. Millhauser, I.J. Pickering, G.N. George, X-ray absorption spectroscopy investigations of copper(II) coordination in the human amyloid β peptide, Inorg. Chem. 58 (9) (2019) 6294–6311.

[107] N. Niimura, R. Bau, Neutron protein crystallography: beyond the folding structure of biological macromolecules, Acta Crystallogr. A 64 (1) (2008) 12–22.

[108] M. Winterer, R. Delaplane, R. McGreevy, X-ray diffraction, neutron scattering and EXAFS spectroscopy of monoclinic zirconia: analysis by Rietveld refinement and reverse Monte Carlo simulations, J. Appl. Crystallogr. 35 (4) (2002) 434–442.

[109] D. Wardecki, D.O. Ojwang, J. Grins, G. Svensson, Neutron diffraction and EXAFS studies of $K_{2x/3}Cu[Fe(CN)_6]_{2/3}\cdot nH_2O$, Cryst. Growth Des. 17 (3) (2017) 1285–1292.

[110] R.A. Scott, J.E. Shokes, N.J. Cosper, F.E. Jenney, M.W.W. Adams, Bottlenecks and roadblocks in high-throughput XAS for structural genomics, J. Synchrotron Radiat. 12 (1) (2005) 19–22.

[111] W. Shi, M. Punta, J. Bohon, J.M. Sauder, R. D'Mello, M. Sullivan, J. Toomey, D. Abel, M. Lippi, A. Passerini, P. Frasconi, S.K. Burley, B. Rost, M.R. Chance, Characterization of metalloproteins by high-throughput X-ray absorption spectroscopy, Genome Res. 21 (6) (2011) 898–907.

[112] K.B. Handing, E. Niedzialkowska, I.G. Shabalin, M.L. Kuhn, H. Zheng, W. Minor, Characterizing metal-binding sites in proteins with X-ray crystallography, Nat. Protoc. 13 (2018) 1062–1090.

[113] P. Dumas, L. Miller, Biological and biomedical applications of synchrotron infrared microspectroscopy, J. Biol. Phys. 29 (2) (2003) 201–218.

[114] L. Miller, Q. Wang, R. Smith, H. Zhong, D. Elliott, J. Warren, A new sample substrate for imaging and correlating organic and trace metal composition in biological cells and tissues, Anal. Bioanal. Chem. 387 (5) (2007) 1705–1715.

[115] X. Xing, R. Du, Y. Li, B. Li, Q. Cai, G. Mo, Y. Gong, Z. Chen, Z. Wu, Structural change of human hair induced by mercury exposure, Environ. Sci. Technol. 47 (19) (2013) 11214–11220.

[116] C. Garino, E. Borfecchia, R. Gobetto, J.A. van Bokhoven, C. Lamberti, Determination of the electronic and structural configuration of coordination compounds by synchrotron-radiation techniques, Coord. Chem. Rev. 277–278 (2014) 130–186.

[117] K. Geraki, M.J. Farquharson, D.A. Bradley, X-ray fluorescence and energy dispersive X-ray diffraction for the quantification of elemental concentrations in breast tissue, Phys. Med. Biol. 49 (1) (2004) 99.

[118] Q.-X. Yuan, B. Deng, Y. Guan, K. Zhang, Y.-J. Liu, Novel developments and applications of nanoscale synchrotron radiation microscopy, Physics 48 (4) (2019) 205–218.
[119] A. Sakdinawat, D. Attwood, Nanoscale X-ray imaging, Nat. Photonics 4 (2010) 840–848.
[120] J. Miao, T. Ishikawa, I.K. Robinson, M.M. Murnane, Beyond crystallography: diffractive imaging using coherent X-ray light sources, Science 348 (6234) (2015) 530–535.
[121] C. Song, H. Jiang, A. Mancuso, B. Amirbekian, L. Peng, R. Sun, S.S. Shah, Z.H. Zhou, T. Ishikawa, J. Miao, Quantitative imaging of single, unstained viruses with coherent X-rays, Phys. Rev. Lett. 101 (15) (2008) 158101.
[122] S.L. Johnson, C.J. Milne, Ultrafast X-ray science: structural transients in solution, Trends Anal. Chem. 29 (6) (2010) 497–507.
[123] C. Wang, U. Steiner, A. Sepe, Synchrotron big data science, Small 14 (46) (2018) 1802291.